Analysis of one-nucleon transfer reactions between heavy ions in terms of exact finite-range distorted-wave Born-approximation calculations

K. S. Low* and T. Tamura
Center for Nuclear Studies,† University of Texas, Austin, Texas 78712
(Received 14 October 1974)

A new technique is developed to carry out exact finite-range distorted-wave Born-approximation calculations very quickly, and is applied to analyze a large amount of data for one-nucleon transfer reactions between heavy ions. It is confirmed that heavy-ion induced reaction data, if analyzed in terms of an exact finite-range approach, can be used as a dependable spectroscopic tool.

[NUCLEAR REACTIONS ^{208}Pb(^{16}O, ^{15}N), E = 104, 140 MeV; ^{208}Pb(^{12}C, ^{11}B), ^{208}Pb(^{12}C, ^{13}C), E = 77, 98, 116 MeV; ^{208}Pb(^{11}B, ^{10}Be), ^{208}Pb(^{11}B, ^{12}B), E = 72.2 MeV; ^{88}Sr(^{16}O, ^{15}N), E = 44–59 MeV; ^{64}Ni(^{16}O, ^{15}N), E = 56 MeV; ^{64}Ni(^{12}C, ^{11}B), E = 48 MeV; calculated $\sigma(\theta)$; full recoil; exact-finite-range DWBA, ^{209}Bi, ^{207}Pb, ^{99}Y, ^{65}Cu levels deduced S.]

I. INTRODUCTION

With the accumulation of experimental data of transfer reactions between heavy ions obtained with ever increasing bombarding energies, the need of carrying out exact finite range (EFR) distorted-wave Born-approximation (DWBA) calculations,[1] which includes recoil effects exactly, has become very evident.[2] The purpose of the present article is to discuss, first, a new technique which allows one to perform EFR-DWBA calculations rather fast, and then to apply this technique to analyze several sets of available data for one-nucleon transfer reactions.

In the past decade, data of light-ion induced direct reactions, analyzed in terms of zero-range DWBA, have been used extensively and efficiently in order to extract nuclear structure information; see, e.g., Ref. 3. The data of heavy-ion induced reactions, if restricted to one-nucleon transfer reactions, may not add very much new insofar as the extraction of structure information is concerned. Nevertheless, an understanding of the mechanism of the heavy-ion induced reaction is of physical interest in itself. Furthermore, once it is confirmed that the one-nucleon transfer reactions induced by heavy ions can be used to extract structure information as reliably as with light-ion induced reactions, it is clear that one can be convinced of the validity of extending the analysis to the multinucleon transfer reactions. We try to supply such a confirmation here. Since such reactions cannot be conceived of within the framework of light-ion induced reactions, it means that the heavy-ion induced reactions open up a completely new way to extract further information on nuclear structure.

In Sec. II we give an expression of the DWBA cross section which is valid for both EFR and no-recoil (NR)[4] approaches. Since there is no evidence of the importance of the spin-orbit interaction in the scattering between two heavy ions this interaction will be ignored throughout the present article, making the expression given in Sec. II extremely simple. Corresponding expressions for the form factor are given in Sec. III, first for EFR calculations following very closely the presentation of Ref. 1, but with slight modification of notation. The form factor for the NR calculation can be obtained as a limiting case of the EFR form factor, and we give only its final form. For a more detailed derivation of the formulas given in Secs. II and III, the reader is referred to Ref. 5.

Section IV is devoted to a brief discussion of the new technique with which the EFR calculations can be carried out very fast. As will be seen, this technique takes full advantage of the fact that the mass of the transferred particle is much smaller than those of the heavy ions between which the transfer takes place. This advantageous situation can sometimes cause inaccuracy in the numerical calculations if it is handled carelessly. Thus, a way to avoid such inaccurate calculations is also given in Sec. IV. Results of numerical calculations are discussed in Sec. V, partly summarizing results which have been reported earlier.[6–8] Final-

ly, Sec. VI gives a discussion concerning the results of the present work and also the prospects of future works.

II. FORMULAS FOR DWBA AMPLITUDES AND CROSS SECTIONS

As is well known[3] the DWBA cross section for a process $A(a,b)B$ is given by

$$\frac{d\sigma^{\mathrm{DWBA}}(\theta)}{dr}=\frac{\mu_a\mu_b}{(2\pi\hbar^2)^2}\frac{k_b}{k_a}\frac{1}{(2I_A+1)(2s_a+1)}\sum_{M_AM_Bm_am_b}|T_{M_Bm_b;M_Am_a}(\theta)|^2, \tag{2.1}$$

with the amplitude

$$T_{M_Bm_b;M_Am_a}=\left(\frac{4\pi}{k_ak_b}\right)\hat{s}_>\hat{I}_>(-)^{I_A-M_A+s_b-m_b+s+m_s}$$

$$\times\sum_{jls}(I_AM_AI_B-M_B|jm_j)(s_am_as_b-m_b|sm_s)(jm_jsm_s|l-m_l)$$

$$\times\hat{l}_a\hat{l}_b(l_a0l_bm_{l_b}|lm_l)(-)^{l_b+m_{l_b}}G_{l_b-m_{l_b}}P_{l_bm_{l_b}}(\theta)I^{jls;AaBb}_{l_b;l_a}. \tag{2.2}$$

Note that $\hat{I}=(2I+1)^{1/2}$ and $G_{lm}=(-)^{(m-|m|)/2}[(l-|m|)!/(l+|m|)!]^{1/2}$, while $(jmj'm'|j''m'')$ is a Clebsch-Gordan (CG) coefficient. Most of the other notation used in (2.1) and (2.2) is rather conventional[1,3] and is easy to understand. We shall thus explain only quantities that are somewhat less obvious.

Note that (2.2) is given in a form[5] which is valid for both stripping and pickup reactions, and the quantities there have the same meaning for both cases except that

$$s_>=s_a,\ s_<=s_b,\ I_>=I_B,\ \text{and}\ I_<=I_A \quad \text{(for stripping)}, \tag{2.3}$$

$$s_>=s_b,\ s_<=s_a,\ I_>=I_A,\ \text{and}\ I_<=I_B \quad \text{(for pickup)}.$$

Further, in (2.2) the dynamical factor $I^{jls;AaBb}_{l_b;l_a}$ is given as

$$I^{jls;AaBb}_{l_b;l_a}=\frac{1}{2l+1}\sum_{m_l}J\int\int d\vec{r}_a d\vec{r}_b\left[\sum_{l_1n_1l_2n_2}d^{jls;AaBb}_{l_1n_1l_2n_2}f^{l_1n_1l_2n_2}_{lm_l}(\vec{r}_1,\vec{r}_2)\right]$$

$$\times(r_ar_b)^{-1}\chi_{l_b}(k_b,r_b)\chi_{l_a}(k_a,r_a)\left[Y_{l_a}(\hat{r}_a)Y_{l_b}(\hat{r}_b)\right]_{lm_l}, \tag{2.4}$$

where $\chi_{l_a}(k_a,r_a)$ and $\chi_{l_b}(k_b,r_b)$ are radial parts of the distorted waves in the incident and exit channels, respectively, while

$$f^{l_1n_1l_2n_2}_{lm_l}(\vec{r}_1,\vec{r}_2)=[\Phi_{l_1n_1}(\vec{r}_1)\Phi_{l_2n_2}(\vec{r}_2)]_{lm}, \tag{2.5a}$$

$$d^{jls;AaBb}_{l_1n_1l_2n_2}=C^{(1)}_{I_>I_<jl_1n_1}C^{(2)}_{s_>s_<sl_2n_2}(-)^{s+l_2-1/2}$$

$$\times W(l_1l_2js;l\tfrac{1}{2}). \tag{2.5b}$$

Note that the choice of the coordinates is made as given in Figs. 1a and 1b, respectively, for stripping and pickup reactions.

In order to explain the notation in (2.5a), let us

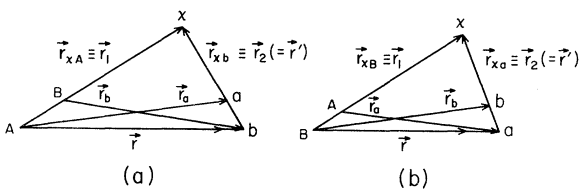

FIG. 1. Choice of coordinates: (a) for pickup and (b) for stripping. The coordinates $\vec{r}_a$, $\vec{r}_b$, $\vec{r}_1$, and $\vec{r}_2$ are used most conveniently for EFR, while $\vec{r}$ and $\vec{r}'$ are for NR calculations.

first consider the amplitude of the stripping reaction given in the post form. Then $\Phi_{l_1 n_1}(\vec{r}_1)$ equals $u_{l_1 n_1}(\vec{r}_1)$, which is the wave function of the nucleon bound to the nucleus A to form B, with the total spin j, the orbital angular momentum l_1, and n_1 radial nodes. Defining $u_{l_2 n_2}(\vec{r}_2)$ in the same way, except that the total spin is denoted as s, we have $\Phi_{l_2 n_2}(\vec{r}_2) = V(r_2) u_{l_2 n_2}(\vec{r}_2)$, where $V(r_2)$ is the potential by which the nucleon is bound to the nucleus b to form a. In (2.5b), for example, $C^{(1)}_{I_B I_A j l_1 n_1}$ is the coefficient of fractional parentage {i.e., the amplitude with which the state [in which the single nucleon in the orbit $(j\, l_1 n_1)$ is coupled to the core nucleus A with spin I_A] is contained in the wave function of B with spin I_B} times $n_j^{1/2}$, where n_j is the number of nucleons in the orbit j in the nucleus A. The meaning of (2.5) in the prior form for the stripping, and also for both forms in the pickup reactions, will be understood similarly.

It is easy to see that the summation over M_A, M_B, m_a, and m_b in (2.1) can be carried out analytically because of the simple form of the CG coefficients in (2.2). The result is given in the following very simplified form:

$$\frac{d\sigma^{\mathrm{DWBA}}(\theta)}{d\Omega} = \frac{\mu_a \mu_b}{(2\pi\hbar^2)^2}\left(\frac{k_b}{k_a}\right)\frac{(2I_>+1)(2s_>+1)}{(2I_A+1)(2s_a+1)}\left(\frac{4\pi}{k_a k_b}\right)^2 S^{(1)}S^{(2)}$$

$$\times \sum_{l m_l}\left|\sum_{l_a l_b} \hat{l}_a \hat{l}_b (l_a 0 l_b m_l \mid l m_l) I^{j l s; Aa Bb}_{l_b; l_a} (-)^{l_b+m_l} G_{l_b -m_l} P_{l_b m_l}(\theta)\right|^2 . \tag{2.6}$$

Note that in (2.6) the product of the spectroscopic factors $S^{(1)}S^{(2)}$, with $S^{(i)} = [C^{(i)}]^2$, has been factored out, where $C^{(i)}$ was introduced in (2.5b). Therefore, in the form of (2.6), the dynamical factor $I^{j l s; AaBb}_{l_b; l_a}$ is to be interpreted to be the same as that in (2.4) except that $C^{(1)}$ and $C^{(2)}$ are replaced by unity in (2.5b). Note also that the possible values of l are those that satisfy the following triangular conditions:

$$\vec{j} + \vec{l} + \vec{s} = 0 \text{ and } \vec{l}_1 + \vec{l}_2 + \vec{l} = 0 . \tag{2.7}$$

We shall make a remark concerning the appearance of the factor $(l_a 0 l_b m_l \mid l m_l) P_{l_b m_l}(\theta)$ in (2.6). As is well known, the characteristic feature of EFR calculations is that the factor $I^{j l s; AaBb}_{l_b; l_a}$ is nonvanishing even if $(-)^{l_a + l_b + l} = -1$. For this parity nonconserving l, however, $(l_a 0 l_b m_l \mid l m_l) = 0$ if $m_l = 0$. This CG coefficient is nonzero for nonzero m_l, but $P_{l_b m_l}(\theta) = 0$ for $\theta = 0$ or $= \pi$, if $m_l \neq 0$. Therefore the contribution to the cross section of the parity nonconserving l still vanishes at these two angles.

III. EXPLICIT REPRESENTATION OF THE FORM FACTOR

The dynamical factor $I^{j l s; AaBb}_{l_b; l_a}$ defined in (2.4) involves a six-dimensional integral, but the integration over the four angular variables can be performed analytically following the procedure developed in Ref. 1. We thus have the dynamical factor in the form of a two-dimensional integral:

$$I^{j l s; Aa Bb}_{l_b; l_a}(\mathrm{EFR}) = J \int\int \chi_{l_b}(k_b, r_b) F^{j l s; AaBb}_{l_b l_a}(r_a, r_b) \chi_{l_a}(k_a, r_a) r_a r_b dr_a dr_b , \tag{3.1}$$

where the form factor is given as

$$F^{j l s; Aa Bb}_{l_b l_a}(r_a, r_b) = \tfrac{1}{2} \sum_{l_1 n_1 l_2 n_2} d^{j l s; AaBb}_{l_1 n_1 l_2 n_2} \sum_k \sum_{\lambda_1 \lambda_1' \lambda_2 \lambda_2' \Lambda_a \Lambda_b} r_a^{\lambda_1 + \lambda_2} r_b^{\lambda_1' + \lambda_2'}$$

$$\times i^{(l_1 + l_2) - (l_a + l_b)} (-)^{k+l} (2k+1) \hat{\lambda}_1 \hat{\lambda}_1' \hat{\lambda}_2 \hat{\lambda}_2' \hat{l}_a \hat{l}_b \hat{\Lambda}_a \hat{\Lambda}_b D_{l_1 \lambda_1 \lambda_1'} D_{l_2 \lambda_2 \lambda_2'} S_1^{\lambda_1} S_2^{\lambda_2} t^{\lambda_1'} l_2^{\lambda_2'}$$

$$\times (\lambda_1 0 \lambda_2 0 \mid \Lambda_a 0)(\lambda_1' 0 \lambda_2' 0 \mid \Lambda_b 0)(\Lambda_a 0 k 0 \mid l_a 0)(\Lambda_b 0 k 0 \mid l_b 0) W(l_a \Lambda_a l_b \Lambda_b; k l)$$

$$\times \begin{Bmatrix} \lambda_1 & \lambda_2 & \Lambda_a \\ \lambda_1' & \lambda_2' & \Lambda_b \\ l_1 & l_2 & l \end{Bmatrix} G_k^{l_1 n_1 l_2 n_2}(r_a, r_b) \tag{3.2}$$

with

$$D_{l\lambda\lambda'} = \delta_{\lambda+\lambda',l}[(2l+1)!/(2\lambda+1)!(2\lambda'+1)!]^{1/2}$$

and the kernel defined by

$$G_k^{l_1 n_1 l_2 n_2}(r_b, r_a) = \int_{-1}^{1} w_{l_1 n_1}(r_1) w_{l_2 n_2}(r_2) P_k(\mu) d\mu \,. \tag{3.3}$$

In (3.3) the function $w_{l_1 n_1}(r_1)$ is the radial part of $\Phi_{l_1 n_1}(\vec{r}_1)$ divided by $r_1^{l_1}$, while $w_{l_2 n_2}(r_2)$ involves another factor $V(r_2)$, the binding potential. Further,

$$r_i = |\vec{r}_i| = |s_i \vec{r}_a + t_i \vec{r}_b| \quad (i = 1, 2), \tag{3.4}$$

and μ in (3.3) is the cosine of the angle between $\vec{r}_a$ and $\vec{r}_b$. Finally, the stripping and pickup cases are distinguished by the following relations:

$$s_1 = aB/xT, \quad t_1 = -bB/xT, \quad s_2 = aA/xT,$$

$$t_2 = -aB/xT, \text{ and } J = (aB/xT)^3 \quad \text{(for stripping)}, \tag{3.5a}$$

$$s_1 = -aA/xT, \quad t_1 = bA/xT, \quad s_2 = -bA/xT,$$

$$t_2 = bB/xT, \text{ and } J = (bA/xT)^3 \quad \text{(for pickup)}. \tag{3.5b}$$

If the calculation is made using (3.1) with (3.2)–(3.5) in (2.6) it may be called an exact finite-range (EFR) calculation since no approximation has been made.

To introduce the NR approximation for the stripping we first express $\vec{r}_a$ and $\vec{r}_b$ as [cf. Fig. 1(a)]

$$\vec{r}_a = \vec{r} + (x/a)\vec{r}' \text{ and } \vec{r}_b = (A/B)\vec{r} + (x/B)\vec{r}' \tag{3.6}$$

and then approximate it as

$$\vec{r}_a = \vec{r} \text{ and } \vec{r}_b = (A/B)\vec{r}\,. \tag{3.7}$$

Then the expression of the dynamical factor is very much simplified, as was shown in detail in Ref. 5. Here we shall show only the results:

$$I_{l_b;l_a}^{jls;AaBb}(\text{NR}) = \frac{A}{B}(\hat{l}_a \hat{l}_b/\hat{l})(l_a 0 l_b 0 | l 0) \int \chi_{l_b}\left(k_b, \frac{A}{B} r\right) F_{\text{NR}}^{jls;AaBb}(r) \chi_{l_a}(k_a, r) dr \,, \tag{3.8}$$

where the NR form factor is given as

$$F_{\text{NR}}^{jls;AaBb}(r) = \tfrac{1}{2} \sum d_{l_1 n_1 l_2 n_2}^{jls;AaBb} r^{\lambda_1} \int r'^{(\lambda_1'+2)} \phi_{l_2 n_2}(r') G_k^{l_1 n_1}(r, r') dr' i^{l_1+l_2-l} (-)^k D_{l_1 \lambda_1 \lambda_1'} \hat{\lambda}_1 \hat{\lambda}_1' \hat{l}_1 \hat{l}_2 (\lambda_1 0 l 0 | k 0)$$

$$\times W(l_1 l_2 \lambda_1 k; l \lambda') \tag{3.9}$$

with

$$G_k^{l_1 n_1}(r, r') = \int_{-1}^{1} w_{l_1 n_1}(|\vec{r} + \vec{r}'|) P_k(\mu) d\mu \,. \tag{3.10}$$

The dynamical factor appropriate for the pickup reaction with NR approximation is given by

$$I_{l_b;l_a}^{jls;AaBb}(\text{NR-pickup}) = \frac{A}{B}(\hat{l}_a \hat{l}_b/\hat{l})(l_a 0 l_b 0 | l 0) \int \chi_{l_b}(k_b, r) F_{\text{RN}}^{jls;AaBb}(r) \chi_{l_a}\left(k_a, \frac{B}{A} r\right) dr$$

$$= \left(\frac{A}{B}\right)^2 (\hat{l}_a \hat{l}_b/\hat{l})(l_a 0 l_b 0 | l 0) \int \chi_{l_b}\left(k_b, \frac{A}{B} r\right) F_{\text{NR}}^{jls;AaBb}\left(\frac{A}{B} r\right) \chi_{l_a}(k_a, r) dr \tag{3.11}$$

IV. REMARKS CONCERNING NUMERICAL CALCULATIONS

The reason why the EFR range calculation is normally so time consuming is that the complicated form factor (3.2) has to be evaluated at *each* mesh point in a huge, multidimensional space, spanned by the quantum numbers j, l, s, l_a, and l_b and also by the (discretized) coordinates r_a and r_b. The number of these mesh points is indeed very large in general, and thus the total number of quantities that are needed to describe the form factor is in the millions. Thus its evaluation, storing, and recovery take much computer time. Note that this number can be particularly large for heavy-ion induced reactions, because they often require usage of rather small mesh size and a wide range for r_a and r_b, as well

as of large numbers of l_a and l_b.

We shall now show that this number of mesh points can be reduced greatly in practice. To see this we first note that the integrand of (3.3) becomes negligibly small if r_1 and/or r_2 exceed their respective critical values R_{1c} and R_{2c}, which can be defined as the radius for which Φ_1 or Φ_2 are six or more orders of magnitude smaller than their peak values. (The actual values of R_{1c} and R_{2c} vary largely from case to case. Very crudely, however, one may say that $R_{2c} \simeq 10$ fm and $R_{1c} \simeq 20-30$ fm.) Therefore, it is necessary to retain in our calculation only pairs of (r_a, r_b) so that $r_i < R_{ic}$ ($i = 1$ and 2) for at least part of the values of μ between -1 and 1. Otherwise G_k and thus F become negligibly small.

The explicit dependence of r_1 and r_2 upon r_a, r_b, and μ can best be seen in the following form, which is obtained from (3.4) with (3.5a) (for stripping):

$$r_1 = \left[\left(\frac{B}{A}\right)^2 (\alpha\delta_{ab} + r_b)^2 + 2\frac{b}{a} r_a r_b \alpha^2(1-\mu)\right]^{1/2}, \tag{4.1a}$$

$$r_2 = \left[(\alpha\delta_{ab})^2 + 2\frac{A}{B} r_a r_b \alpha^2(1-\mu)\right]^{1/2}, \tag{4.1b}$$

where

$$\alpha = \frac{aB}{x(a+A)} \quad \text{and} \quad \delta_{ab} = \frac{A}{B} r_a - r_b . \tag{4.2}$$

In (4.2) we note that α is large (being equal, e.g., to approximately 12 and 16 for (^{12}C, ^{11}B) and (^{16}O, ^{15}N) reactions on ^{208}Pb, respectively) and that r_a and r_b are also large, being at least equal to the lower cutoff radius R_{ic} (about 8 fm in the two reactions mentioned). Then, in order to keep $r_i < R_{ic}$, the following restrictions can be imposed upon r_a, r_b, and μ: (i) $|\delta_{ab}|$ must be kept very small, e.g. $|\delta_{ab}| < 1$ fm, and (ii) μ must be kept very close to unity in order to make $\alpha^2(1-\mu) \lesssim 1$.

What the restriction (i) implies is that the region in the (r_a, r_b) space in which F is to be calculated is confined within a very narrow band along the line defined by $\delta_{ab} = 0$, i.e. the (diagonal) line $r_b = (A/B) r_a \simeq r_a$. This reduces drastically the number of mesh points that must be calculated.

The restrictions (i) and (ii) together result in another important property that, for a given set of δ_{ab} and μ, both r_1 and r_2 depend very weakly on r_b. Therefore G_k and consequently F depends very weakly on r_b for a fixed value of δ_{ab}. Thus, if we take the mesh size for δ_{ab} to be Δ and calculate F for r_b (for each fixed δ_{ab}) with a mesh size equal to $n\Delta$ ($n > 1$), the values of F at the intermediate $(n-1)$ points can then be obtained by interpolation. Because of the weak dependence of F on r_b, the needed accuracy for F is not lost this way while its speed of evaluation is increased by a factor of n. Our experience showed that n can be taken as large as 10, although it depends on the value of Δ.

Further, the restriction (ii) can be used in speeding up the evaluation of the integral in (3.3). Note that $P_k(\mu)$ for a large k is a highly oscillatory function if it is considered in the whole range of μ from -1 to 1. However, if $P_k(\mu)$ is considered only in the range of μ from $\mu_{\min} \simeq 1 - \alpha^{-2} \simeq 0.99$ to unity, it is not very oscillatory. Therefore, even when G_k has to be calculated up to a very large value of k, the number of mesh points (e.g. with the Gaussian quadrature) to be taken for μ in performing the integral in (3.3) accurately can be much smaller than k, allowing this integration to be carried out very rapidly.

We shall now make a remark which is not particularly related to speeding up the numerical calculations, but rather to guaranteeing in an important way sufficient accuracy in evaluating the form factor for EFR calculations. Let us first note that the form factor (3.2) involves manyfold summations, and that in the summand the parameters s_1, s_2, t_1, and t_2 are all large, being of the order of $\alpha \simeq 16$, if we again use the example of the ^{208}Pb(^{16}O, ^{15}N)^{209}Bi reaction. Therefore the value of the factor $s_1^{\lambda_1} s_2^{\lambda_2} t_1^{\lambda'_1} t_2^{\lambda'_2}$ ($\equiv F_1$) in the summand is about $16^{\lambda_1+\lambda_2+\lambda'_1+\lambda'_2} = 16^{l_1+l_2} = 16^5 \simeq 10^6$, if the $\frac{9}{2}^-$ state in ^{209}Bi is considered (i.e. if $l_1 = 4$ and $l_2 = 1$), which is a very large value.

The most important contribution to the integral of (3.1) is expected to come from the values of $r_a \approx r_b \approx R$, where R is of the order of magnitude of the channel radius $r_0(a^{1/3} + A^{1/3}) \simeq r_0(b^{1/3} + B^{1/3})$, r_0 being the radius parameter of the optical potential. Therefore, in the summand of (3.2) the other factor $r_a^{\lambda_1+\lambda_2} r_b^{\lambda'_1+\lambda'_2}$ ($\equiv F_2$) is of the order of magnitude of $R^{l_1+l_2}$. As can be seen from the derivation[1,5] of (3.2), however, the origin of the combined factor F_1F_2 is the factor $r_1^{l_1} r_2^{l_2}$ which is again of the order of $R^{l_1+l_2}$. It is thus seen that, if the order of magnitude of G_k is written as $O(G_k)$, the order of magnitude of the right-hand side of (3.2), after all the summations are taken, must be of the order of $R^{l_1+l_2} O(G_k)$: On the other hand, that of each summand is $10^6 R^{l_1+l_2} O(G_k)$. In other words, the complicated geometric factor in (3.2), whose magnitude is of the order of unity, has a very specific phase relation which *cancels out drastically* the contributions of individual summands to the sum.

This drastic cancellation means that, if one wants to obtain the form factor with an accuracy of 5 significant figures, say, each summand in (3.2) must be obtained with 11 significant figures.

TABLE I. Optical model parameter (OMP) sets.

Set No.	V (MeV)	W (MeV)	r_0 (fm)	a (fm)	Origin Ref.
OMP-I	40	15	1.310	0.45	9
OMP-II	40	15	1.218	0.612	10
OMP-III	100	25	1.210	0.50	11
OMP-IV	100	25.81	1.223	0.50	8
OMP-V	120	15.02	1.203	0.50	8

Note, however, that the summand has G_k as a factor, and it is not an easy task to obtain it with this high accuracy.

It is not difficult, however, to evaluate the factor F_1F_2 so that it carries 11 significant figures. Therefore, the best route to follow would be to perform first the summations over λ_1, λ_2, λ_1', λ_2', Λ_a, and Λ_b, so that the evaluation of the square-bracket factor of (3.2) is completed *before* it is multiplied by G_k. As the above argument shows, this square-bracket factor is of the order of $R^{l_1+l_2}$, and carries 5 significant figures. In the final summation over k in (3.2), it is thus clear that the sum and the summands are of the same order of magnitude, and thus any serious further loss of accuracy is not expected to take place in the carrying out of this summation. In other words, if G_k is obtained with 5 significant figures, which is an easy task, it is guaranteed that the form factor is obtained with the same accuracy.

V. RESULTS OF NUMERICAL CALCULATIONS

We analyzed various data for single-nucleon transfer reactions in terms of EFR-DWBA calculations, and the results of these calculations will be summarized here.

As is seen below, there is available a fairly large amount of data obtained by taking ^{208}Pb as target, and the motive for choosing this target is obvious. It is a doubly magic nucleus, and thus the final states formed by one-nucleon transfer reactions are expected to be (almost) purely single-particle states. The analysis of such data can therefore be considered as a good test for the validity of a theory used for the analysis. The results of our analyses show that EFR-DWBA is indeed a valid theoretical tool, while NR-DWBA is not.

It should be noted that any experiment which uses a heavy nucleus like ^{208}Pb as a target has to be carried out with a high incident energy, since otherwise the Coulomb barrier cannot be overcome and thus the cross section will be immeasurably small. Theoretically, this means that the calculations have to be made including a large number of partial waves. Also the upper cutoff radius in the integral (3.1) has to be taken very large (≈30 fm), particularly when the process is that of the stripping of a proton onto ^{208}Pb, where the nucleon in the residual nucleus is very weakly bound because of the doubly magic nature of ^{208}Pb. It is thus seen that the calculations are rather involved in general. With the method developed in Sec. IV, however, such calculations were performed with comparative ease.

TABLE II. Spectroscopic factors S_2 for pairs of smaller nuclei. They are theoretical values given in Ref. 12.

Nuclear pair	^{16}O-^{15}N	^{13}C-^{12}C	^{12}C-^{11}B	^{12}B-^{11}B	^{11}B-^{10}Be
S_2	2.00	0.613	2.85	0.708	0.43

Not only data with ^{208}Pb as target but also data with many other targets were analyzed. As is seen below, the targets that are chosen cover a wide range of the periodic table, and EFR-DWBA is found to work well for all the data. The sets of optical parameters used in these calculations are summarized in Table I, where references from which these sets were taken are also given.

The values of $S^{(2)}$(i.e., the spectroscopic factor normally denoted as C^2S) between pairs of lighter ions involved in the reactions considered below are summarized in Table II. They are theoretical values of Cohen and Kurath.[12] Using these values and fitting the theoretical cross section to experiment, the spectroscopic factor $S^{(1)}$ for the heavier system can be extracted. In the following, this $S^{(1)}$ will be denoted as S_{EFR} or S_{NR} depending on whether it is extracted from EFR or NR calculations.

All the calculations to be presented below were performed by using the computer program SATURN-MARS-1 (SM1).[13] Most of the experimental data to be discussed below had been analyzed previously by using the same program and the results were reported elsewhere,[6-8] but unfortunately a not very systematic use of bound state and optical parameters was made in these works. We thus have reanalyzed most of the data and the results summarized below were obtained this way.

Throughout this work, the wave function of the transferred nucleon was obtained by using the separation energy procedure with the Woods-Saxon potential. A fixed set of parameters $r_0 = 1.20$ fm, $a = 0.65$ fm, and (the strength of the spin-orbit interaction) $V_{so} = 7$ MeV, to be called BS-0, is used for lighter systems. For heavier systems, particularly for ^{208}Pb and ^{209}Bi, different sets are used and they are listed in Table III as sets BS-1 through BS-4.

TABLE III. Bound state (BS) parameter sets.

Set No.	r_0 (fm)	a (fm)	V_{so} (MeV)	r_{so} (fm)	a_{so} (fm)	Origin Ref.
BS-0	1.20	0.65	7	1.20	0.65	...
BS-1	1.28	0.76	...	...	...	6
BS-2	1.28	0.76	6	1.09	0.60	14
BS-3	1.28	0.76	7	1.28	0.76	9
BS-4	1.28	0.63	7	1.10	0.50	15

It would be in order here to comment on the numerical accuracy of our calculations, concerning which one might have doubts because of the use of interpolation introduced below Eq. (4.2) in Sec. IV. Our experience shows that, so long as the basic mesh size Δ (also defined in Sec. IV) is as small as 0.04–0.07 fm, to set $n=10$, i.e., to use 10 point interpolation, does not cause any significant error. In order to show that a high accuracy is indeed maintained, we give in Table IV differential cross sections at several angles for the case of ^{88}Sr(^{16}O, ^{15}N)^{89}Y with $E_{lab}(^{16}O)=59$ MeV. (The values given there were obtained by assuming that $S_1S_2=1$.) As is seen, the resultant cross section at the peak (70°) varies only within 0.3% when n is varied from 3 to 10. The situation is the same at 10°, 40°, and 120° where the cross sections are two to three orders of magnitude smaller than the peak value. The error is noticeable only at 170° where the cross section is four orders of magnitude smaller than the peak value. It will further be seen in Table IV that, for practical purposes, to use $n=15$ or even 20 may be permissible. It is thus clear that one can indeed use interpolation without losing accuracy, and make the calculation much faster and easier than otherwise. Table IV also shows a result with LOLA,[16] and our calculation agrees with this result within a small fraction of a percent.

In spite of the accuracy with which we made calculations, we have been informed by several independent workers (see e.g. Ref. 16) that their own calculations did not agree with our results reported earlier.[6,7] We have since found that this apparent disagreement resulted simply from the use of different parameters in their calculations from those we used; and further that this confusion was caused by a few erroneous and/or vague statements we made about the parameters used in our previous calculations. We shall itemize here such erroneous statements and thus clarify the situation.

(i) In the caption of Fig. 1 of Ref. 6, we stated that $V_{so}=6$ MeV was used to describe the protons bound in ^{209}Bi. Actually the S_1 values given in Table I of this reference were obtained by setting $V_{so}=0$. (ii) As was stated in the caption of Fig. 1

TABLE IV. Differential cross sections for ^{88}Sr(^{16}O, ^{15}N)^{89}Y($p_{1/2}$) reaction for $E_{lab}(^{16}O)=59$ MeV with $l=0$ only. Results with various Δ and n are given.

	Cross sections in mb/sr				
$\Delta=0.05$ fm n	10° $\times10^{-4}$	40° $\times10^{-3}$	70° $\times10^{-1}$	120° $\times10^{-3}$	170° $\times10^{-5}$
3	2.578	3.895	3.592	2.657	6.525
6	2.576	3.903	3.590	2.636	6.641
10	2.592	3.889	3.579	2.640	5.246
15	2.745	3.927	3.535	2.670	5.831
20	2.533	3.760	3.444	2.471	3.972
25	2.611	3.608	3.220	2.046	11.640
$\Delta=0.1$ fm $n=5$	2.875	4.092	3.892	2.826	5.338
LOLA (Ref. 16)			3.585		

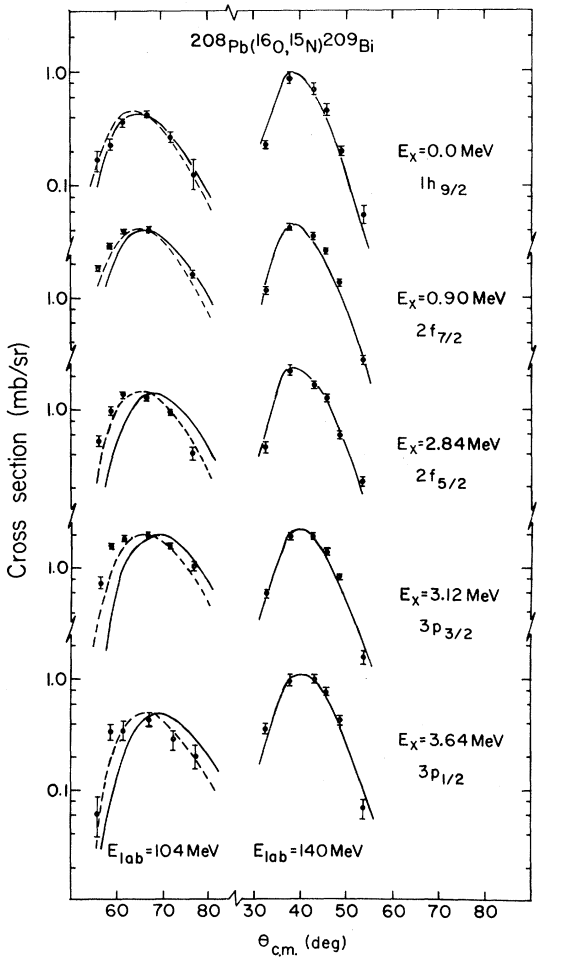

FIG. 2. Comparison with experiment of the ^{208}Pb(^{16}O, ^{15}N)^{209}Bi reaction (Ref. 9). The solid lines were obtained by using OMP-I (the optical parameter set No. I) of Table I, for both channels, while the dotted lines were obtained by using $r_0=1.35$ fm in the exit channel.

of Ref. 7, $V_{so}=6$ MeV was indeed used in calculating the wave functions of the bound protons. However, this spin-orbit interaction was ignored in the transition operator [i.e., in the binding potential $V(r_2)$ defined below Eq. (3.3)]. (iii) In the caption of Table I of Ref. 7, we stated that $C^2S=2.85$ was used for the system ^{12}C-^{11}B. The actual value used was $C^2S=2.44$. (iv) Concerning the calculation for the reaction $^{88}Sr(^{16}O, ^{15}N)^{89}Y$ reported very briefly in Ref. 6, no information was given concerning the bound state parameters. The values used there were $r_0=1.20$ fm, $a=0.65$ fm, and $V_{so}=7$ MeV for ^{89}Y, while the same set, except that $a=0.60$ fm, was used for ^{16}O. As was the case in (ii) above, V_{so} was not included in $V(r_2)$ used as a transition operator.

The time t needed to perform an EFR-DWBA with SM1 is approximately

$$t = c l_{\max} n_{\mathrm{mes}} \sum (2l+1), \tag{5.1}$$

where $l_{\max}$ is the maximum value of the orbital angular momentum in the distorted wave, n_{mes} is the number of mesh points (with the mesh size Δ) in the radial integral, and in the last factor of (5.1) l is the transferred orbital angular momentum. With a CDC-6600 computer $c \approx 0.0001$ sec, while if IBM360/195 is used c is reduced by about a factor of 3.

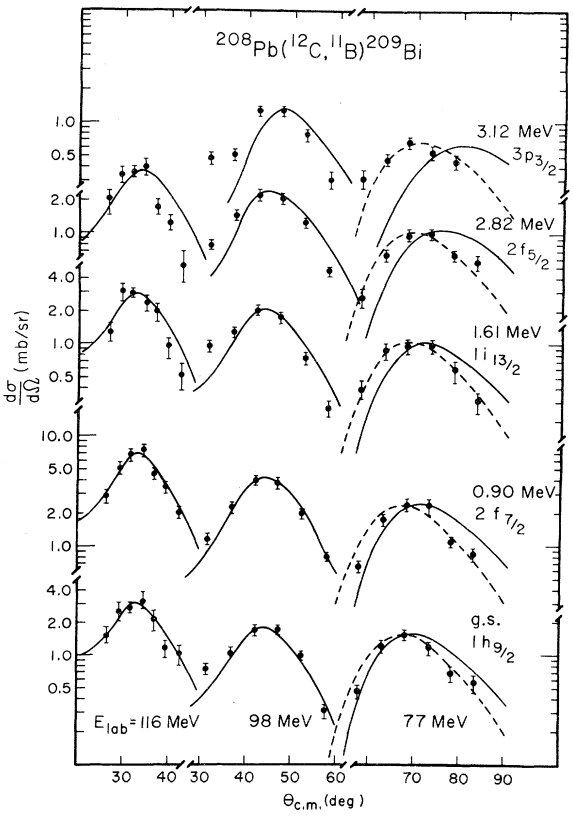

FIG. 3. Comparison with experiment of the $^{208}Pb(^{12}C, ^{11}B)^{209}Bi$ reaction (Ref. 17). The solid lines were obtained by using OMP-II, while the dotted lines were obtained by taking $r_0=1.38$ fm in the exit channel.

A. Reactions stripping one-proton onto ^{208}Pb

The available experimental data falling under this category are those of $(^{16}O, ^{15}N)$, $(^{12}C, ^{11}B)$ and $(^{11}B, ^{10}Be)$ reactions reported in Refs. 9, 17, and 18, respectively. Among them, the data for $(^{16}O, ^{15}N)$ reaction were taken with the laboratory energy E_{lab} of the projectile equal to 104 and 140 MeV, while those of the $(^{12}C, ^{11}B)$ reaction were taken with $E_{\mathrm{lab}}=77$, 98, and 116 MeV. Finally the

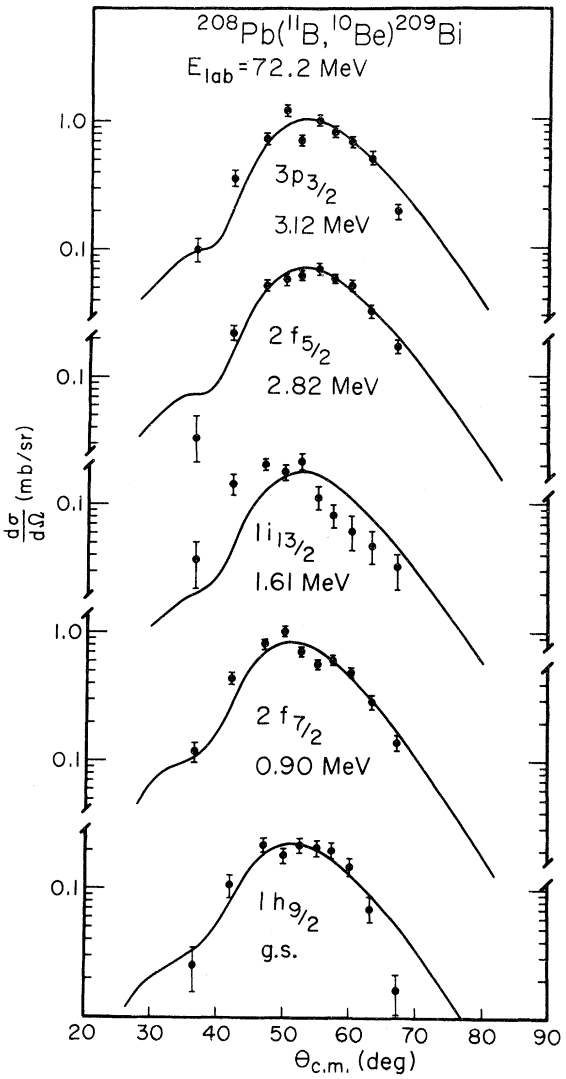

FIG. 4. Comparison with experiment of the $^{208}Pb(^{11}B, ^{10}Be)^{209}Bi$ reaction (Ref. 18). All the theoretical curves were obtained by using OMP-II.

TABLE V. Results of the EFR calculations for the ^{208}Pb(^{16}O, ^{15}N)^{208}Bi reaction. OMP-I was used throughout.

			E_{lab} = 104 MeV					E_{lab} = 140 MeV					Comparison		
			S_{EFR}			S_{NR}[a]	$\sigma_{L'}/\sigma_L$	S_{EFR}			S_{NR}[a]	$\sigma_{L'}/\sigma_L$	S_{EFR} (average over E_{lab})		
E_x (MeV)	nlj	L,L'	BS-1[d]	BS-2	BS-3	BS-3	BS-1	BS-1[d]	BS-2	BS-3	BS-3	BS-1	BS-2	(^{3}He, d)[b]	Theory[c]
0.00	$1h_{9/2}$	4, 5	1.05 (1.50)	1.20	1.60	3.04	0.14	1.00	1.07	1.45	3.84	0.20	1.14	1.17	0.95
0.90	$2f_{7/2}$	4, 3	0.82 (1.03)	0.81	0.80	0.80	0.03	0.72	0.71	0.69	0.48	0.08	0.76	0.78	0.85
1.61	$1i_{13/2}$	7, 6	0.70 (0.84)	0.68	0.64	0.66	0.02	0.56	0.53	0.48	0.40	0.07	0.61	0.56	0.70
2.84	$2f_{5/2}$	2, 3	0.75 (0.88)	0.81	0.98	3.20	0.10	0.57	0.58	0.70	3.20	0.17	0.70	0.88	0.66
3.12	$3p_{3/2}$	2, 1	0.65 (0.68)	0.66	0.68	0.92	0.02	0.55	0.56	0.59	0.48	0.06	0.61	0.67	0.74
3.64	$3p_{1/2}$	0, 1	0.50 (0.50)	0.54	0.59	2.80	0.15	0.65	0.68	0.75	4.80	0.34	0.61	0.45	0.54

[a] Taken from Ref. 9.
[b] Taken from Ref. 20.
[c] Taken from Ref. 22.
[d] Taken from Ref. 6.

data of the (^{11}B, ^{10}Be) reaction were taken only with E_{lab} = 72.2 MeV.

The comparison of the theoretical cross sections with the data is made in Figs. 2–4 and the spectroscopic factors extracted by using the fit in these figures are given in Tables V–VII, and are also displayed in Fig. 5.

As is seen, the fit of the angular distribution (given by solid lines) is very good for the higher E_{lab} in both (^{16}O, ^{15}N) and (^{12}C, ^{11}B) reactions, but gets somewhat poorer for the lowest E_{lab} and with increased excitation energy E_x of the final states in ^{209}Bi. As the curves given in Figs. 2 and 3 with dotted lines show, however, one can get a satisfactory fit to the data if the radius parameter in the exit channel is increased slightly from what it is in the incident channel.

Note that, for example, the peak position of the angular distribution of the (^{12}C, ^{11}B) reaction given by the solid lines in Fig. 3 for E_{lab} = 77 MeV shifts to larger angles as E_x increases, while there is a much weaker shift for higher E_{lab}. We shall first present a general discussion on why this behavior is seen, particularly when the angular distribution is basically bell-shaped as is the case here.

In order to explain this feature, let us denote as l_{ag} (l_{bg}) the angular momentum corresponding to the classical grazing collision in the incident (exit) channel. Then it is expected that if the triangular condition $\vec{l}_{ag} + \vec{l}_{bg} + \vec{l} = 0$ is satisfied, the peak position approximately coincides with the grazing angle

TABLE VI. Results of the EFR calculations for the ^{208}Pb(^{12}C, ^{11}B)^{209}Bi reaction.

		BS-2											
		OMP-I E_{lab} (MeV)			OMP-II E_{lab} (MeV)			S_{EFR} (Average over E_{lab}) OMP-I		OMP-II		Comparison	
E_x (MeV)	nlj	77	98	116	77	98	116	BS-2	BS-3[c]	BS-2	BS-3[c]	(^{3}He, d)[a]	Theory[b]
0.00	$1h_{9/2}$	1.21	0.88	1.15	0.54	0.37	0.46	1.08	1.42	0.47	0.57	1.17	0.95
0.90	$2f_{7/2}$	1.26	1.12	1.30	0.58	0.47	0.54	1.23	1.13	0.53	0.49	0.78	0.85
1.61	$1i_{13/2}$	1.18	1.09	1.01	0.52	0.47	0.43	1.09	0.89	0.47	0.39	0.56	0.70
2.82	$2f_{5/2}$	0.90	0.85	0.87	0.42	0.36	0.37	0.87	1.07	0.38	0.46	0.88	0.66
3.12	$3p_{3/2}$	1.50	1.35	d	0.74	0.57	d	1.42	1.41	0.66	0.65	0.67	0.74
3.64	$3p_{1/2}$	1.21[e]	d	d	0.59	d	d	1.21	1.32	0.59	0.64	0.45	0.54

[a] Taken from Ref. 20.
[b] Taken from Ref. 22.
[c] These values are essentially 0.77 times those given in Table I of Ref. 7.
[d] No data available.
[e] E_{lab} = 78 MeV data of Ref. 9 were used.

TABLE VII. Results of the EFR calculations for the ^{208}Pb(^{11}B, ^{10}Be) reaction at 72.2 MeV. BS-2 was used throughout.

E_x (MeV)	nlj	S_{EFR} OMP-I	OMP-II [a]	(^{3}He, d) [b]	Theory [c]
0.00	$1h_{9/2}$	1.04	0.47	1.17	0.95
0.90	$2f_{7/2}$	0.99	0.51	0.78	0.85
1.61	$1i_{13/2}$	1.06	0.60	0.56	0.70
2.82	$2f_{5/2}$	0.76	0.35	0.88	0.66
3.12	$3p_{3/2}$	1.09	0.58	0.67	0.74

[a] These S values were taken from Ref. 10. Note that the bound state parameter used for ^{11}B there had $r_0 = 1.35$ fm, $a = 0.50$ fm, and $V_{so} = 7$ MeV.

[b] Taken from Ref. 20.

[c] Taken from Ref. 22.

in the incident channel. However, if l_{bg} is much smaller than l_{ag}, which occurs for example when the Q value is negative and large as is the case in the ^{208}Pb(^{12}C, ^{13}C)^{207}Pb reaction discussed in Sec. V B, the above triangular condition is violated. Then l_{ai}, the value of l_a which contributes most importantly to the reaction, is smaller than l_{ag} and the peak shifts to a larger angle. As E_x increases, Q values become more negative and the peaks shift to still larger angles. Note also that the total real potential, i.e. the sum of the (real part of the) nuclear, Coulomb, and centrifugal potentials for $l_a \simeq l_{ag}$, when plotted as a function of r_a, has a dip in the surface region even for E_{lab} as large as 77 MeV; see Fig. 6. Thus a slight deviation of l_{ai} from l_{ag} will cause a large shift of the peak position. However, if E_{lab} increases the value of l_{ag} also increases, and the dip in the corresponding total potential almost disappears. This fact and the fact that the ratio $(l_{ag} - l_{ai})/l_{ag}$ gets smaller explains why the shift of the peak gets smaller with increased E_{lab}.

Compared with the (^{12}C, ^{13}C) reaction, the Q value is much more negative in the (^{12}C, ^{11}B) reaction, but its effect is to some extent compensated for by the lowering of the Coulomb potential in the exit channel resulting in about the same l_{bg} as before. Thus, it is expected that the behavior of the peak position in the (^{12}C, ^{11}B) reaction will still be very much the same as in the (^{12}C, ^{13}C) reaction, and the result presented by the solid lines in Fig. 3 shows that such an expectation is fulfilled. Sur-

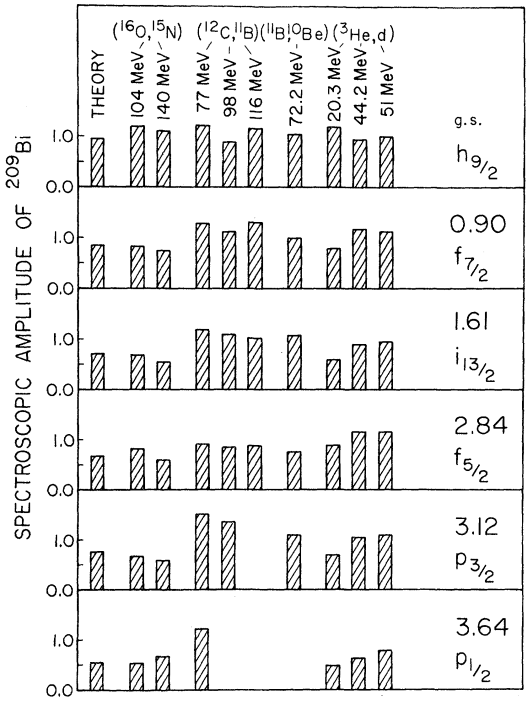

FIG. 5. Summary of S_{EFR} values for states in ^{209}Bi, extracted from various reactions and various sets of parameters.

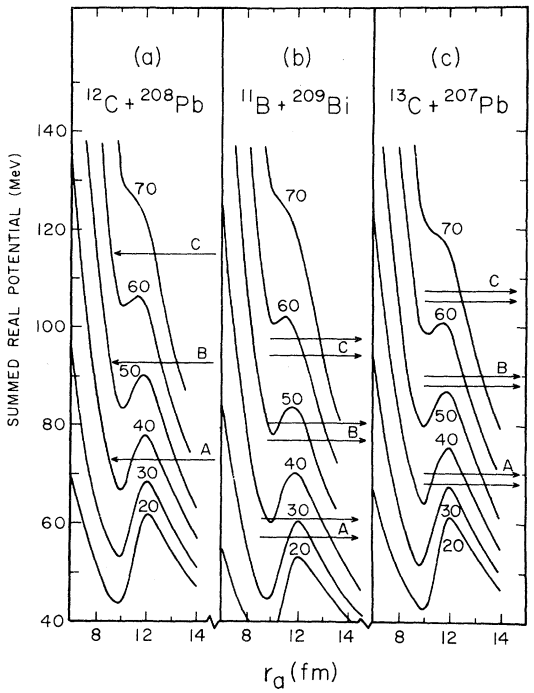

FIG. 6. Sum of the real part of the nuclear potential (OMP-I of Table I), the Coulomb potential, and the centrifugal potentials. The angular momentum of different partial waves are labeled on each curve: (a) is for the incident channel, while (b) and (c) are for the exit channels in the reactions ^{208}Pb(^{12}C, ^{11}B)^{209}Bi and ^{208}Pb(^{12}C, ^{13}C)^{207}Pb. Three energies, E_{lab}(^{12}C) = 77, 98, and 116 MeV, were considered, which were labeled as A, B, and C, respectively, in the figure. For the exit channels, two energy lines, corresponding to the lowest and highest states of ^{209}Bi and ^{207}Pb considered in the text, are drawn.

prisingly enough, however, the experimental angular distribution does not show such a shift, and thus we get discrepancy.

From what we argued above, one expects that the peak position for lower E_{lab} depends sensitively upon the detail shape of the dip in the total potential, and thus upon the optical parameters. The improved fit obtained in Figs. 2 and 3 with the dotted lines indeed shows that there is a room for searching for parameters other than those we used in obtaining the solid lines.

It is remarkable to see in Table V that the spectroscopic factor S_{EFR} extracted by fitting the ^{208}Pb-(^{16}O, ^{15}N)^{209}Bi data with EFR-DWBA is essentially independent of E_{lab}. Note further that S_{EFR} is very close to unity for the ground $\frac{9}{2}^-$ state, and decreases smoothly with decreasing j to 0.5 for the $\frac{1}{2}^-$ state. This feature is at variance with a previous (h, d) study[19] which gave $S \approx 1$ for all j, though another (h, d) work[20] of which results are reproduced in our Table V extracted S in about the same way as it is in our result. It should be noted that lower spin states are highly excited states, and thus are likely to lose more of their single-particle nature. In fact, recent structural studies[21,22] predicted $S(\frac{9}{2}) \simeq 1$ and $S(\frac{1}{2}) \simeq 0.5$ and it thus appears that our results are very reasonable. The fact that $S(\frac{13^+}{2}) \simeq 0.5$ is also reasonable, because this state is expected to be about a 50-50 mixture of a single-particle $i_{13/2}$ state and the core-excited $(3^- \times \frac{9}{2}^-)_{13/2^+}$ state.[21] As is seen in Table V, S_{NR} obtained with the NR approximation[9] is not only E_{lab} dependent, but also shows a very strong dependence on the $j > (j = l + \frac{1}{2})$ and $j < (j = l - \frac{1}{2})$ nature of the final state, contradicting EFR results.

In comparing EFR and NR calculations, it should be noted further that the EFR cross section σ (EFR) can be written as a sum of σ_L and $\sigma_{L'}$, the

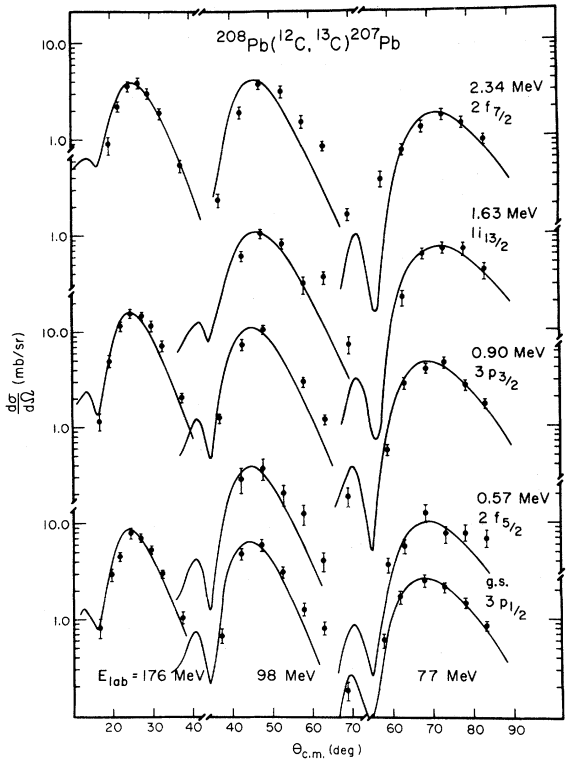

FIG. 7. Comparison with experiment of the ^{208}Pb-(^{12}C, ^{13}C)^{207}Pb reaction (Ref. 17). All the theoretical curves were obtained by using OMP-I.

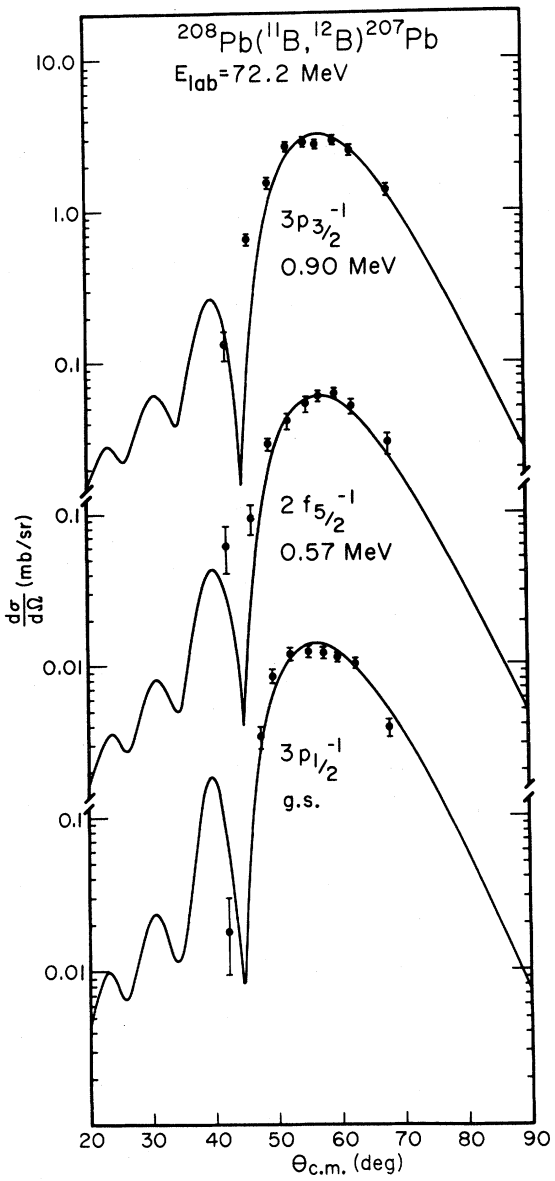

FIG. 8. Comparison with experiment of the ^{208}Pb(^{11}B, ^{10}B)^{207}Pb reaction (Ref. 18). All the theoretical curves were obtained by using OMP-II.

TABLE VIII. Spectroscopic factors for states of ^{207}Pb.

E_x (MeV)	nlj	(^{12}C, ^{13}C) BS-4, OMP-I E_{lab} (MeV) 77	98	116	Average	BS-3, OMP-I Average	(^{11}B, ^{12}B) BS-4 OMP-I	OMP-II	(d,t) [a]	(h,α) [b]	Theory [c]
0.00	$3p_{1/2}$	1.60	1.71	1.72	1.68	1.17	2.54	1.73	1.00	1.00	0.95
0.57	$2f_{5/2}$	1.38	1.77	d	1.58	1.19	2.90	1.93	1.00	0.63	0.94
0.90	$3p_{3/2}$	1.22	1.55	1.97	1.58	0.95	2.48	1.58	0.85	1.00	0.92
1.64	$1i_{13/2}$	1.10	1.29	d	1.20	0.63	d	d	0.71	0.63	0.87
2.34	$2f_{7/2}$	0.93	1.09	0.88	0.97	0.54	d	d	0.75	0.75	0.70

[a] Taken from Ref. 23.
[b] Taken from Ref. 24.
[c] Taken from Ref. 22.
[d] No data available.

contributions of components with transferred orbital angular momentum L and L' of a natural and unnatural parity nature, respectively. The values of L and L' are listed in Table V, which also gives the ratio $\sigma_{L'}/\sigma_L$. Since this ratio, which vanishes for NR, is comparatively small even for EFR, it is seen that the large difference between S_{EFR} and S_{NR} must arise from the difference between σ_L(EFR) and σ_L(NR); and in fact we get, e.g. for the 104 MeV case, σ_L(EFR/σ_L(NR)=2.5, 0.7, 1.9, 0.5, and 1.3 for $j=\frac{1}{2}$ through $\frac{9}{2}$. This example shows how dangerous the NR calculation can be, even when $\sigma_{L'}/\sigma_L$ as estimated with EFR calculations is rather small.

Table VI presents S_{EFR} for states in ^{209}Bi that were extracted by fitting the ^{208}Pb(^{12}C, ^{11}B)^{209}Bi data given by the solid lines in Fig. 3. It is seen that, if the parameters OMP-I and BS-2 are used, the values for lower excited states are about the same as those given in the last three columns of Table V, but those for higher excited states are somewhat too large. We do not know at this moment why such discrepancy takes place, although it could be due to the deformation of the nuclei ^{12}C and ^{11}B. Table VI also presents values of S_{EFR} obtained by using OMP-II and BS-2, and it is seen that the values of these new S_{EFR} are about half those with OMP-I, presenting an example of the sensitivity of S upon the optical parameters. Table VI further gives results with BS-3, with the intent of showing the dependence on the bound state parameters, and, as is seen, there appears a rather erratic $j_>$ and $j_<$ dependence of the extracted S values.

The values of S_{EFR} obtained by fitting the (^{11}B, ^{10}Be) data as seen in Fig. 4 are given in Table VII. Their behavior with respect to the choice of OMP-I and OMP-II is about the same as in the case of (^{12}C, ^{11}B) reactions.

The solid lines given in Fig. 4 fit the data very well for all the states, in spite of the fact that $E_{lab}=72.2$ MeV is lower than the lowest energy $E_{lab}=77$ MeV in the case of (^{12}C, ^{11}B) reaction. The reason is that the Coulomb barrier in the (^{11}B, ^{10}Be) reaction is much lower than that in the (^{12}C, ^{11}B) reaction, and thus a given E_{lab} in the former corresponds to a higher E_{lab} in the latter.

The S_{EFR} corresponding to the dotted lines in Fig. 2 are given in parentheses in Table V. Their values differ as much as about 50% from those corresponding to solid lines, indicating that, in spite of the good fit to the angular distribution, the *ad hoc* increase we made of the radius or diffuseness parameters in the exit channel might not be a correct approach, and thus a more careful search of optical parameters is needed. It may also indicate the need of investigating the contributions of processes which are more complicated than that described by simple DWBA.

Finally, Fig. 5 is presented so as to make easy the comparison of various entries in Tables V–VII. After a detailed discussion about these tables, no additional comment will be needed for this figure.

TABLE IX. Spectroscopic factor S_{EFR} and S_{NR} for states of ^{89}Y. BS-0 was used for both ^{16}O and ^{89}Y.

E_{lab} (MeV)	0.91 MeV $1g_{9/2}$ S_{EFR}	S_{NR} [a]	g.s. $2p_{1/2}$ S_{EFR}	S_{NR} [a]	$S(p_{1/2})/S(g_{9/2})$ EFR	NR [a]
44	1.16	1.58	1.15	1.67	1.0	1.03
46	1.70	2.29	1.99	3.01	1.17	1.29
48	1.71	1.94	2.09	3.23	1.22	1.63
52	1.69	1.94	1.91	3.23	1.13	1.63
56	1.61	1.67	2.02	3.29	1.25	1.93
59	1.83	1.76	2.32	3.89	1.27	2.16
Average [b]	1.71	1.92	2.07	3.33	1.23	1.73
(h,d) [c]	0.88		0.90		1.02	

[a] Taken from Ref. 11.
[b] Values for $E_2=44$ MeV were excluded.
[c] Taken from Ref. 25.

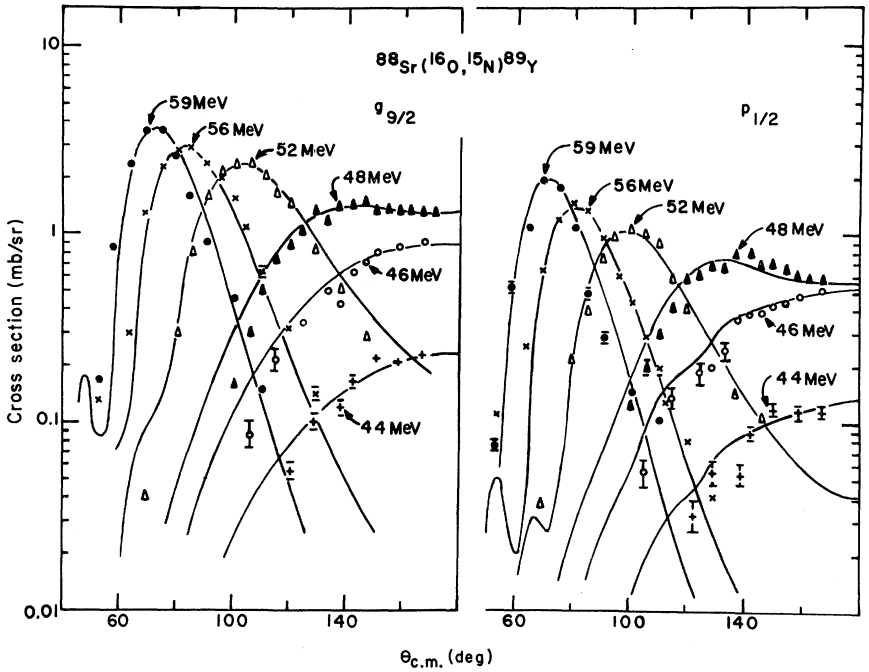

FIG. 9. Comparison with experiment of the ^{88}Sr(^{16}O, ^{15}N)^{89}Y reaction (Ref. 11). All the theoretical curves were obtained with OMP-III.

B. Reactions picking up one neutron from ^{208}Pb

The available experimental data falling under this category are those of the (^{12}C, ^{13}C) and (^{11}B, ^{12}B) reactions reported, respectively, in Refs. 17 and 18. The values of E_{lab} used for these reactions were the same as those for the (^{12}C, ^{11}B) and (^{11}B, ^{10}Be) reactions discussed in Sec. V A.

As is seen in Figs. 7 and 8, the theoretical angular distribution obtained by using OMP-II fits the experiment very well for both reactions and for all the energies in the case of (^{12}C, ^{13}C) reaction. (Somewhat poorer fits to the $\frac{7}{2}^-$ state in ^{207}Pb with E_{lab} = 98 MeV might be due to the poor quality of the data.) The reason why good agreement was obtained even for the lowest E_{lab} (=77 MeV) for the (^{12}C, ^{13}C) reaction is that the experimental peak shifted to larger angles with increased E_x, as the theory leads one to expect (this is emphasized in Sec. V A).

The spectroscopic factors S_{EFR} for states in ^{209}Pb extracted from the fits obtained in Figs. 7 and 8 are given in Table VIII, and are seen to be in good accord with those extracted from light-ion induced reactions.[23,24]

C. ^{88}Sr(^{16}O, ^{15}N)^{89}Y reaction

The experiment on the ^{88}Sr(^{16}O, ^{15}N)^{89}Y reaction by Anantaraman[11] is interesting in that the measurement was made at six values of E_{lab} ranging from 44 to 59 MeV. As is seen in Fig. 9, the angular distribution for the lowest two energies peaks at 180°, a characteristic feature for the sub-Coulomb reaction. With increasing E_{lab} the peak moves away from 180°, and at the highest energies the angular distributions display typical bell shape.

As is seen in the figure, the EFR cross section fits the data very well for all the six energies considered, although an almost equally good fit was obtained even when the calculation was made with the NR approximation,[4] as is seen in Figs. 6 and 7 of Ref. 11. Notice, however, the slight wiggle that appears in the $p_{1/2}$ curves for E_{lab} = 44 and 46 MeV in our Fig. 9, which is missing in the corresponding curves of Ref. 11, possibly caused by a crude plotting of the curves. The origin of this wiggle lies in the fact that a smaller number of partial waves contribute to the sub-Coulomb reaction. This feature is expected to be less pronounced the larger the transferred l value, and that is the likely reason why the corresponding wiggle did not appear in the $g_{9/2}$ angular distribution.

In spite of the good NR fit to the angular distributions, the NR prediction of the magnitude has a difficulty similar to that encountered in the ^{208}Pb-(^{16}O, ^{15}N)^{209}Bi reaction. As was shown in Ref. 11, the extracted spectroscopic factor S_{NR} for the $p_{1/2}$ final state increased by about a factor of 2 in going

TABLE X. Values of S_{EFR} and S_{NR} for states of ^{65}Cu.

E_x	nlj	L	(^{12}C, ^{11}B) NR	(^{12}C, ^{11}B) EFR	L	(^{16}O, ^{15}N) NR	(^{16}O, ^{15}N) EFR	(h,d) [a]	(α,t) [b]
0.00	$2p_{3/2}$	0, 1, 2	0.79 (0.63)	0.79 (0.51)	1, 2	0.79 (1.05)	0.79 (1.01)	0.79	0.79
0.77	$2p_{1/2}$	1, 2	0.53 (0.42)	0.61 (0.40)	0, 1	1.19 (1.58)	0.70 (0.89)	0.75	1.00
1.11	$1f_{5/2}$	2, 3, 4	0.34 (0.27)	0.37 (0.24)	2, 3	1.03 (1.38)	0.42 (0.54)	0.26	0.38
1.48	$1f_{7/2}$	2, 3, 4	0.054(0.43)	0.054(0.035)	3, 4	0.054(0.072)	0.054(0.067)	0.054	•••
1.62	$1f_{5/2}$	2, 3, 4	0.69 (0.56)	0.73 (0.47)	2, 3	2.07 (2.75)	0.78 (1.00)	0.57	0.91
2.51	$1g_{9/2}$	3, 4, 5	0.67 (0.54)	0.57 (0.37)	4, 5	0.58 (0.69)	0.54 (0.69)	0.29	0.35
	N		0.80 (1.00)	0.65 (1.00)		1.33 (1.00)	1.28 (1.00)		

[a] Taken from Ref. 26.

[b] Taken from Ref. 27.

from 44 to 59 MeV. This trouble disappears in S_{EFR} as is seen in Table IX (except for the value for 44 MeV, which might be caused by the experimental difficulty in calibrating the effective E_{lab} at this low energy; see the note added in proof in Ref. 11).

The energy averaged S_{EFR}, which equals 2.07 and 1.71, respectively, for the $p_{1/2}$ and $g_{9/2}$ states, differ from the values 0.90 and 0.88 extracted for these two states from the ^{88}Sr$(h, d)^{89}$Y reaction,[25] but this may simply indicate that the bound state parameter set BS-0, used not only for ^{16}O but also for ^{89}Y, is not adequate for the latter.

D. Reactions stripping one proton onto ^{64}Ni

The data considered here are of (^{16}O, ^{15}N) and (^{12}C, ^{11}B) reactions, and a fairly detailed account of their analyses was already given elsewhere.[8] We shall therefore summarize them very briefly here.

The fit to the experimental angular distribution in terms of both NR and EFR calculations are given in Figs. 10 and 11, and the values of S_{NR} and S_{EFR} extracted from this fit are given in Table X.

As is seen, two sets of S values are given in this table, the ones without parentheses being those obtained by multiplying the right-hand side of Eq. (2.6) with an extra normalization factor N so as to make $S = 0.79$ for the ground $\frac{3}{2}^-$ state, in accord with the value obtained from light-ion induced reactions.[26,27] Other sets given in parentheses are those obtained without extra normalization, i.e. with $N = 1$.

It is seen that S_{EFR} without parentheses for both reactions agree fairly well with the light-ion values, but a rather large discrepancy is seen in S_{NR}, particularly those extracted from the (^{16}O, ^{15}N) reaction for $j_<$ states. This discrepancy is much more marked when $N = 1$ is taken.

In spite of the good mutual agreement of the normalized S_{EFR} values extracted from the (^{16}O, ^{15}N) and (^{12}C, ^{11}B) reactions, the unnormalized S_{EFR} differ from each other by about a factor of 2. Note that a similar but somewhat less pronounced discrepancy was seen in the comparison of the S_{EFR} values extracted from (^{16}O, ^{15}N) and (^{12}C, ^{11}B) reactions from ^{208}Pb. We shall discuss this problem in the next section.

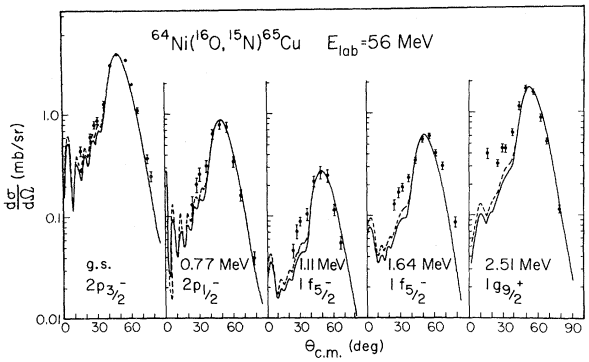

FIG. 10. Comparison with experiment of the ^{64}Ni(^{16}O, ^{15}N)^{65}Cu reaction (Ref. 8). The solid (dashed) lines are EFR (NR) results. All these curves were obtained by using OMP-IV, except that $a = 0.60$ fm in the exit channel.

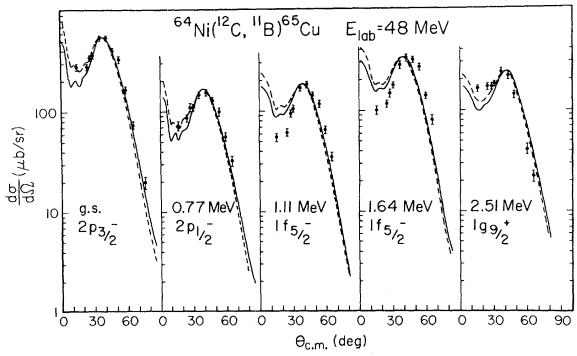

FIG. 11. Comparison with experiment of the ^{64}Ni(^{12}C, ^{11}B)^{65}Cu reaction (Ref. 8). The solid (dashed) lines are EFR (NR) results. All these curves were obtained by using OMP-V except that $a = 0.60$ fm in the exit channel.

VI. CONCLUDING REMARKS

From the results summarized in Sec. V one may say rather safely that the EFR analysis of the one-nucleon transfer reactions between heavy ions allows one to extract spectroscopic factors within a factor of 2 in the absolute magnitude, and possibly much better, particularly when relative magnitudes are concerned. It is also gratifying to see that the extraction of the spectroscopic factor can be made independent of $E_{\rm lab}$, because then data obtained with a variety of accelerators can be used with equal significance. Since, furthermore, it has been established that using our techniques the EFR calculation takes only a few times more computer time than needed in performing NR calculations, the EFR analysis can be made on a more or less routine basis. It thus appears that heavy-ion induced transfer reaction data can in fact be used as a very useful spectroscopic tool.

As was seen in Sec. V, one of the most serious sources of ambiguity in extracting $S_{\rm EFR}$ is the lack of sufficient knowledge of optical parameters. Accumulation of more scattering data and their optical model (and/or coupled-channel) analyses are needed in order to make full use of available and forthcoming data for transfer reactions.

We pointed out at the end of Sec. V D that $S_{\rm EFR}$ extracted from (^{16}O, ^{15}N) and (^{12}C, ^{11}B) reactions differs by as much as a factor of 2. This may again simply be due to the lack of sufficient knowledge of optical parameters. Another conceivable, and probably more interesting, possibility is, however, that the difference between the nuclear shape of ^{12}C and ^{11}B on the one hand and of ^{16}O and ^{15}N on the other, is responsible for this difference: The former pair of nuclei are well deformed, while the latter pair are spherical. If this is indeed the case, it would mean that EFR-CCBA (coupled-channel Born-approximation) calculations rather than EFR-DWBA are needed to analyze (^{12}C, ^{11}B) data, and in fact we are now engaged in such calculations. It should be noted that with the same projectile having a given deformation β, the effective deformation $\beta_{\rm eff} = \beta a^{1/3}/(a^{1/3}+A^{1/3})$ that is to be used in the CCBA calculation gets smaller as the target mass A increases. It is thus very interesting to reemphasize the fact that the difference between the (^{16}O, ^{15}N) and (^{12}C, ^{11}B) spectroscopic factors was much more pronounced when ^{64}Ni was used as target than it was when ^{208}Pb was used as target.

Note added in proof: In Sec. V A we discussed, referring to Figs. 3 and 4, the discrepancy between the peak positions of the theoretical (solid lines) and the experimental angular distributions for lower E_L. In this regard let us consider the effect of the two-step process, in which an inelastic scattering to excite a (collective) state in ^{208}Pb precedes the proton transfer. The l_{ai} for this two-step process is somewhat smaller than the l_{ai} ($= l_{ai}^{(1)}$) for the one-step process. Therefore, if the two processes interfere destructively the net l_{ai} will become larger than $l_{ai}^{(1)}$, and thus the peak position is shifted to a smaller angle, in agreement with experiment. Such an effect has indeed been observed in our recent work, in which the above kind of inelastic effect was included.[28]

ACKNOWLEDGMENTS

The present work was initiated while we stayed at the Argonne National Laboratory in the academic year 1973/74. We are very much indebted to the Argonne Associated Universities which made our stay there possible. We cordially thank many experimentalists and theorists at the Physics Division, Argonne National Laboratory, for their generous help and hearty encouragement. Helpful communications with many other experimentalists, in particular Dr. J. L. C. Ford, Jr., Dr. D. G. Kovar, Dr. M. C. Mermaz, and Dr. K. S. Toth, are acknowledged. We also thank Dr. T. Udagawa for many useful discussions as well as Dr. W. R. Coker for a careful reading of this manuscript. Finally, and not the least, we thank Dr. R. M. DeVries for several stimulating discussions and communications.

---

*Present address: Department de Physique Nucléaire, Centre d'Etudes Nucléaires de Saclay, Saclay, France.

†Work supported in part by the U.S. Atomic Energy Commission.

[1]N. Austern, R. M. Drisco, E. C. Halbert, and G. R. Satchler, Phys. Rev. 133, B3 (1964).

[2]R. Bock and H. Yoshida, Nucl. Phys. A189, 177 (1972); R. DeVries and K. Kubo, Phys. Rev. Lett. 30, 325 (1973).

[3]N. Austern, *Direct Nuclear Reaction Theories* (Wiley, New York, 1970).

[4]P. J. A. Buttle and L. J. B. Goldfarb, Nucl. Phys. 78, 409 (1966); T. Sawaguri and W. Tobocman, J. Math. Phys. (N.Y.) 6, 2223 (1967); F. Schmittroth, W. Tobocman, and A. A. Golestaneh, Phys. Rev. C 1, 377 (1970).

[5]T. Tamura, Phys. Rep. 14, 59 (1964).

[6]T. Tamura and K. S. Low, Phys. Rev. Lett. 31, 1356 (1973).

[7]K. S. Low and T. Tamura, Phys. Lett. 48B, 285 (1974).

[8]A. Cunsulo, M. C. Lemaire, M. C. Mermaz, H. Sztark, K. S. Low, and T. Tamura, Phys. Rev. C 10, 180 (1974).

[9]D. G. Kovar, B. G. Harvey, F. D. Becchetti, J. Mahoney, D. L. Hendrie, H. Homeyer, W. von Oertzen, and M. A. Nagarajan, Phys. Rev. Lett. 30, 1075 (1973).
[10]G. R. Satchler, private communication; J. L. C. Ford, Jr. *et al.*, Phys. Rev. C 10, 1429 (1974).
[11]N. Anantaraman, Phys. Rev. C 8, 2245 (1973).
[12]S. Cohen and D. Kurath, Nucl. Phys. A101, 1 (1967).
[13]T. Tamura and K. S. Low, Comp. Phys. Comm. (to be published).
[14]C. J. Batty and G. N. Greenlees, Nucl. Phys. A133, 673 (1969).
[15]M. Dost, W. R. Hering, and W. R. Smith, Nucl. Phys. A93, 357 (1967).
[16]J. S. Blair, R. M. DeVries, K. G. Nair, A. J. Baltz, and W. Reisdorg, Phys. Rev. C 10, 1856 (1974); R. M. DeVries, private communication.
[17]J. S. Larsen, J. L. C. Ford, Jr., R. M. Gaedke, K. S. Toth, J. B. Ball, and R. H. Hahn, Phys. Lett. 42B, 205 (1972).
[18]J. L. C. Ford, Jr., K. S. Toth, D. C. Hensley, R. M. Gaedke, P. J. Riley, and S. T. Thorton, Argonne National Laboratory Physics Division Informal Report No. PHY-1973B, 1973 (unpublished), p. 495.
[19]B. H. Wildenthal, B. M. Preedom, E. Newmana, and M. R. Cates, Phys. Rev. Lett. 19, 960 (1967).
[20]C. Ellegarrd and P. Vedelsby, Phys. Lett. 26B, 155 (1968).
[21]I. Hamamoto, Nucl. Phys. A141, 1 (1970); and unpublished.
[22]P. Ring and E. Werner, Nucl. Phys. A211, 198 (1973).
[23]W. C. Parkinson, D. L. Hendrie, H. H. Duhm, J. Mahoney, J. Saundinos, and G. R. Satchler, Phys. Rev. 178, 1967 (1969).
[24]W. P. Alford and D. G. Burke, Phys. Rev. 185, 1560 (1969).
[25]J. Picard and G. Bassani, Nucl. Phys. A131, 636 (1969).
[26]A. G. Blair, Phys. Rev. 140, B648 (1965).
[27]M. Gaillard, R. Bouche, L. Feuvrais, P. Gaillard, A. Guichard, M. Gusakow, J. L. Leonhardt, and J. P. Pizzi, Nucl. Phys. A119, 161 (1968).
[28]K. Yagi, D. L. Hendrie, L. Kraus, C. F. Maguire, J. Mahoney, D. K. Scott, Y. Terrien, T. Udagawa, K. S. Low, and T. Tamura, Phys. Rev. Lett. 34, 96 (1975).